Human cone light adaptation: From behavioral measurements to molecular mechanisms

Andrew Stockman Institute of Ophthalmology, University College London, London, UK

Micha Langendörfer Forschungsstelle für Experimentelle Ophthalmologie, Tübingen, F.R.G.

Hannah E. Smithson Department of Psychology, University of Durham, Durham, UK

Lindsay T. Sharpe Institute of Ophthalmology, University College London, London, UK

The ability of the cone visual system to regulate its sensitivity from twilight to bright sunlight is an extraordinary feat of biology. Here, we investigate the changes in visual processing that accompany cone light adaptation over a 5 $\log_{10}$ unit intensity range by combining measures of temporal sensitivity made in one eye with measures of the temporal delay *between* the two eyes in different states of adaptation. This combination of techniques, which provides more complete information than has been available before, leads to a simple model of steady-state light adaptation. At high light levels, visual sensitivity is maintained mainly by photopigment bleaching. At low-to-moderate light levels, it is maintained by trading unwanted sensitivity for speed and by an additional process that paradoxically *increases* the overall sensitivity as the light level rises. Each stage of the model can be linked to molecular mechanisms within the photoreceptor: The speeding up can be linked to faster rates of decay of activated molecules; the paradoxical sensitivity increases can be linked to faster rates of molecular resynthesis and to changes in channel sensitivity; and the sensitivity decreases can be linked to bleaching. Together, these mechanisms act to maintain the cone visual system in an optimal operating range and to protect it from overload.

Keywords: light adaptation, photopic, cones, temporal sensitivity, phase lags, protanopes, sensitivity regulation, visual transduction

Introduction

Despite the limitations imposed by the individual neurons in the visual pathway, many of which have dynamic ranges of no more than circa 10^2 from the level of noise to their response ceiling (e.g., Barlow & Levick, 1976; Shapley & Enroth-Cugell, 1984), the human visual system is able to operate over a $>10^{11}$ range of environmental light levels. It does this in part by depending on a more sensitive rod-driven *scotopic* subsystem at low levels and on a less sensitive cone-driven *photopic* subsystem at high levels (Parinaud, 1881; Schultze, 1866; von Kries, 1894, 1896). Within each subsystem, mechanisms of adaptation act to maintain the system within an optimal operating range as the illumination level is increased. In this article, we investigate the mechanisms of photopic light adaptation.

A fundamental characteristic of human cone light adaptation is that the visual response speeds up as the light level increases, so that under bright conditions, observers become relatively more sensitive to flicker at higher temporal frequencies. Such changes are typically investigated by determining the dependence of temporal modulation sensitivity on temporal (flicker) frequency at different light levels (e.g., De Lange, 1958; Green, 1968; Kelly, 1961b, 1974; Roufs, 1972a). Modulation-sensitivity data (or their reciprocal, modulation threshold data), however, provide only a partial picture of the effects of light adaptation. A complete picture requires knowledge of the accompanying reductions in visual delay (e.g., Cavonius & Estévez, 1980; Lit, 1949; Pulfrich, 1922; Rock & Fox, 1949; Wilson & Anstis, 1969). Here, we combine measures of phase delay and sensitivity obtained over an extensive range of adaptation levels.

Modulation sensitivities can be measured directly. Perceptual delays, however, must be measured relative to the response of a second process, the adaptive state of which can be independently controlled. Although hard to achieve monocularly, such control can be easily achieved binocularly by presenting lights of different intensity to the two eyes. Intraocular delays can then be measured using a binocular flicker-cancellation technique, which relies on the well-established observation that binocular

doi: 10.1167/6.11.5 Received April 17, 2006; published October 18, 2006 ISSN 1534-7362

flicker is phase dependent and that different phases of flicker in the two eyes can destructively interfere (e.g., Baker, 1952a, 1952b, 1952c, 1952d; Baker & Bott, 1951; Cavonius, 1979; Cavonius & Estévez, 1980; Ireland, 1950; Perrin, 1954; Sherrington, 1906; Thomas, 1954, 1955, 1956).

For adaptation to protect the photopic visual system from overload as the light level increases, the primary mechanisms of sensitivity regulation must be early in the visual pathways, most likely in the human cone photoreceptors themselves (see below, and Boynton & Whitten, 1970; Burkhardt, 1994; Valeton & van Norren, 1983). And, indeed, we find that it is possible to relate our results not only to models based on photoreceptor recordings (e.g., Baylor & Hodgkin, 1974; Baylor, Hodgkin, & Lamb, 1974; Fuortes & Hodgkin, 1964; Penn & Hagins, 1972) but also to specific molecular mechanisms operating in the phototransduction cascade (e.g., Pugh, Nikonov, & Lamb, 1999).

Phototransduction and the molecular mechanisms of light adaptation

The phototransduction cascade and the molecular mechanisms of sensitivity regulation are covered in several excellent reviews (see Arshavsky, Lamb, & Pugh, 2002; Burns & Baylor, 2001; Fain, Matthews, Cornwall, & Koutalos, 2001; Perlman & Normann, 1998; Pugh & Lamb, 2000; Pugh et al., 1999). Briefly, the absorption of a photon initiates vision by isomerizing the chromophore molecule, 11-*cis*-retinal, to its all-*trans* form, which rapidly causes a conformational change of the G-protein-coupled receptor-protein cone opsin (R) into the activated photoproduct R* (or metarhodopsin II). R* in turn activates the heterotrimeric G-protein transducin trimer (Gα-GDP-G$\beta\gamma$) by catalyzing the exchange of GDP for GTP, which initiates the separation of the activated α-transducin (Gα* or Gα-GTP) from the trimer. Gα* then activates the effector molecule, phosphodiesterase enzyme (PDE6*), which reduces the cytoplasmic concentration of cGMP by catalyzing its hydrolysis into GMP. The reduction in cGMP concentration results in the closure of the cyclic-nucleotide-gated (CNG) channels in the plasma membrane, which block the inward flow of Na^+ and Ca^{2+} ions, precipitating membrane hyperpolarization and the initialization of the neural response.

Psychophysical models and molecular mechanisms

When interpreting psychophysical data at the molecular level, it is convenient to categorize the molecular mechanisms according to their likely effects on modulation-sensitivity and phase-delay measurements. One category (Category A) is composed of mechanisms that are likely to speed up the visual response and shorten the visual integration time and, thus, alter sensitivity in a way that depends upon temporal frequency. Potential mechanisms are: (i) the increase in the rate of cGMP hydrolysis mediated by the light-induced rise in the concentration of PDE6* (Hodgkin & Nunn, 1988; Nikonov, Engheta, & Pugh, 1998) and (ii) the decrease in the lifetime of R* mediated by rhodopsin kinase (RK; Fain, Lamb, Matthews, & Murphy, 1989; Gray-Keller & Detwiler, 1996; Matthews, 1996, 1997; Murnick & Lamb, 1996; Torre, Matthews, & Lamb, 1986; Whitlock & Lamb, 1999). A second category (Category B) comprises mechanisms that are likely to *reduce* overall sensitivity independently of temporal frequency and are likely to have little effect on phase delay. Potential mechanisms are: (i) pigment bleaching (e.g., Boynton & Whitten, 1970; Burkhardt, 1994; Hecht, 1937) and (ii) response compression caused by the availability of fewer CNG channels as the light level increases (Baylor & Hodgkin, 1974; Dowling & Ripps, 1970; Matthews, Murphy, Fain, & Lamb, 1988). Lastly, a third category (Category C) contains mechanisms that are likely to *increase* overall sensitivity in a way that does not depend on temporal frequency and probably have little effect on phase delay. Potential mechanisms are: (i) the increase in the rate of cGMP synthesis mediated by guanylyl cyclase (Hodgkin & Nunn, 1988; Koutalos, Nakatani, Tamura, & Yau, 1995; Koutalos, Nakatani, & Yau, 1995; Koutalos & Yau, 1996; Polans, Baehr, & Palczewski, 1996; Pugh, Duda, Sitaramayya, & Sharma, 1997; Tamura, Nakatani, & Yau, 1991) and (ii) the decrease in $K_{1/2}$ (the half-activation concentration) for cGMP opening the CNG channels, which has the effect of making more channels available (Bauer, 1996; Chen et al., 1994; Grunwald, Yu, Yu, & Yau, 1998; Hsu & Molday, 1993, 1994; Rebrik & Korenbrot, 1998; Weitz et al., 1998).

Several psychophysical models incorporate mechanisms of Type A that shorten the integration time and/or Type B that attenuate or desensitize the visual response (see the Discussion section, and for reviews, see Graham & Hood, 1992; Hood, 1998; Hood & Finkelstein, 1986; MacLeod, 1978; Shapley & Enroth-Cugell, 1984). Attenuation or desensitization of Type B is also known as von Kries adaptation (von Kries, 1902), or multiplicative scaling, and has been likened to putting on dark glasses (MacLeod, 1978) because all lights and temporal frequencies are equally attenuated. No models, until now, however, have incorporated mechanisms of Type C, which amplify or sensitize the response, because these are counter to the conventional belief that as light level increases, sensitivity must decrease.

The question of how our eyes are able to respond to light over the enormous range of illumination encountered in the environment, while simultaneously optimizing discrimination in space and time, has fascinated scientists for almost a quarter of a millennium (Bouguer, 1760; Fechner, 1860). Here, we address this question by measuring temporal modulation thresholds and temporal

phase delays in two observers over more than 5 $\log_{10}$ units of intensity. On the basis of our new results, we propose a simple model of steady-state adaptation with two intensity-dependent parameters that can be plausibly linked to the underlying molecular mechanisms.

Methods

Subjects

Two male subjects, M.L. and M.M., served as observers in these experiments. Both were protanopic when tested with a standard Nagel Type I anomaloscope (i.e., they could match spectral lights in the red–green range by adjusting only the relative intensities of the lights). The molecular genetics reveal that M.L. has two genes in the opsin gene array on his X chromosome that produce photopigments with essentially identical spectral sensitivities (e.g., Merbs & Nathans, 1992; Sharpe et al., 1998). M.M. is known to have more than one gene in the array (Nathans, personal communication), but we do not know his exact genotype. According to Carroll, Neitz, Hofer, Neitz, and Williams (2004), who have also used M.M. as a subject: "MM is an example in which the L-pigment gene has been replaced by a gene encoding an M pigment, both the first and second gene in his array encode M pigments."

Apparatus

A five-channel binocular Maxwellian-view optical system was used to project the stimuli directly on the observer's retinae. All five channels originated from a 900-W xenon arc lamp, run at constant current, which enabled the production of very intense stimuli. Three of the channels had their beams focused in the observer's left pupil, and two were focused in his right pupil. The images of the arc in the observer's pupils were less than 2 mm in diameter. Because these images were smaller than the smallest natural pupil, the effective light levels were unaffected by one of the other mechanisms of light adaptation, namely, pupillary constriction and dilation. Test and field wavelengths were selected by the use of 3-cavity, blocked interference filters with half-maximum bandwidths of between 7 and 11 nm (Ealing or Oriel). The channels seen by the eyes were optically isolated from each other.

A variable, circular neutral density wedge (Rolyn Optics), mounted on a computer-controlled stepping motor, was positioned in each channel to control radiance. Fixed neutral density filters (Inconel) could also be placed in the beams as required. Circular field stops were used to define the sizes of the test and adapting fields.

Three optical channels contained fast liquid crystal light valves (Displaytech, LC050CP). Sinusoidal temporal waveforms were produced by pulse width modulating the light valves around a carrier frequency of 400 Hz (which is too fast to be perceptually resolved, so that subjects saw only the sinusoidal intensity variation produced by the pulse-width modulation). The contrast of the shutters measured in situ was better than 300:1 at wavelengths longer than 500 nm. Each shutter had rise and fall times of less than 50 μs and could produce sinusoidal modulations from 0% to 92%. Each was driven by computer-controlled programmable timers.

Calibration

The radiant fluxes of the test and adapting fields were measured daily at the plane of the observer's entrance pupil with a radiometer (Graseby Electronics), which had been cross-calibrated with comparable devices traceable to U.S. and German national standards. Interference filters were spectrally calibrated in situ with a spectroradiometer (Gamma Scientific).

Experimental conditions

Modulation threshold measurements

Modulation thresholds were measured monocularly at each of the luminance levels noted in the left column of Figure 1. A 4° diameter, 610-nm target was superimposed in the center of a larger, 9° diameter, 540-nm background and presented only to the left eye. This combination of target and background wavelengths and luminances was chosen to eliminate flicker detection by the S-cones and to saturate the rods. The ratio of the time-averaged radiance of the smaller disc to the radiance of the larger disc was fixed: The larger background was always six times more intense for the M-cones than the target. Thus, the maximum possible M-cone modulation under all conditions was 13%. Modulation was adjusted by varying the modulation of the 610-nm target. The 540-nm background remained steady. The luminances noted in Figure 1 and below are the time-averaged luminances of the *combined* target and background.

At the three lowest background luminances (which are below rod saturating levels), no differences were found between measurements made during the cone plateau following a 99% rod bleach and those made after complete dark adaptation, which indicates that rods play no role in these experiments. The 9° diameter, 500-nm rod bleaching light was produced by the fifth optical channel.

Phase lag measurements

In these binocular experiments, the target and field stimuli seen by the left eye were identical to those used to measure

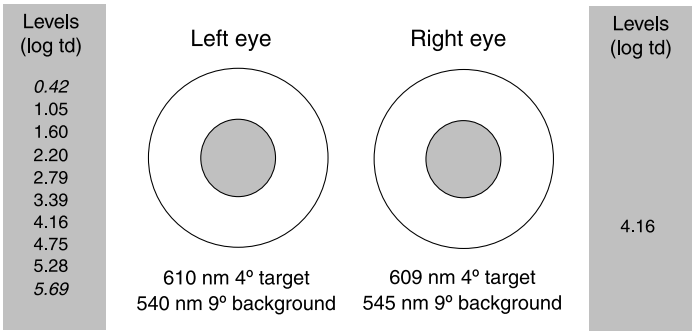

Figure 1. Stimulus configuration and adaptation levels. Only the left eye stimuli were used for the modulation threshold measurements. Both the left and the right eye stimuli were used for the phase-delay measurements. The levels are given in log photopic trolands and are for the combined target and background; those in italics were presented only to the primary observer M.L.

modulation thresholds (see Figure 1): A 4° diameter, 610-nm target was superimposed in the center of a larger, 9° diameter, 540-nm background, and their levels were again set so that the 540-nm background was six times more intense for the M-cones than was the 610-nm target. The stimuli seen by the right eye were essentially the same: A 4° diameter, 609-nm target was superimposed in the center of a 9° diameter, 545-nm background. Their levels were also set so that the background was six times more intense for the M-cones than was the target. For protanopes, the slight differences in wavelength, which arose because different interference filters were used in different channels, are trivial. The maximum M-cone modulation under all conditions was 13% for both left and right eye stimuli.

Once again, a 9° diameter, 500-nm rod bleaching light was used to check that rods were not contributing to flicker detection at the lowest target radiances used in the left eye.

Experimental procedures

Subjects interacted with the computer-controlled Maxwellian-view optical system by means of an eight-button keypad and received instructions and information from the computer by means of tones and a voice synthesizer. The observers light adapted to the target and background fields for at least 3 min prior to any data collection. Temporal frequencies used were multiples of 2.5 Hz.

Modulation threshold measurements

Modulation thresholds were measured by the method of adjustment. Modulation, which is defined as $(I_{max} - I_{min})/(I_{max} + I_{min})$, is given in terms of M-cone excitation. Relative cone excitations were calculated using the Stockman and Sharpe (2000) cone spectral sensitivities. An alternative way of specifying threshold is in terms of the flicker amplitude, which is simply the difference between I_{max} and I_{min}. Amplitudes are given in units of log trolands.

To determine modulation threshold, the subject was presented with the flickering stimulus and asked to adjust its modulation until the flicker appeared just at threshold. On a single run, three threshold settings were made at each temporal frequency. The data are averaged from five (M.L.) or three (M.M.) separate runs.

Phase lag measurements

Phase lags were measured using an extension of flicker photometry, in which the subject was instructed to vary the relative phase as well as the modulation of the two binocularly fused targets to abolish or minimize the subjective flicker. By pressing keys, the subject could advance or retard the phase in large or small steps or flip the phase by 180°. If the region of the null covered an extended range of phase delays, which was usually the case if one of the two signals was weak, subjects were instructed to set the middle of the range.

Three phase settings were made at each temporal frequency in a single experimental run. At least five (M.L.) or three (M.M.) separate experimental runs were carried out for each condition.

The principle behind using phase adjustments to measure relative perceptual delays is illustrated in Figure 2 and described in the figure legend.

Results

Simplified human model

To simplify the data and their interpretation, we confined the detection of our stimuli to the middle-wavelength sensitive (M-) cones by the use of experimental conditions that eliminated any short-wavelength sensitive (S-) cone contribution and by the use of two color-deficient observers, known as "protanopes," who lack long-wavelength sensitive (L-) cones. Had we used color normals, our results would have reflected the separate adaptation of the L- and M-cones and their pathways and would have been complicated by the sometimes substantial phase differences that can arise between flicker signals generated by the L- and M-cone photoreceptors (e.g., Smith, Lee, Pokorny, Martin, & Valberg, 1992; Stockman & Plummer, 2005a, 2005b; Stockman, Plummer, & Montag, 2005; Stromeyer et al., 2000).

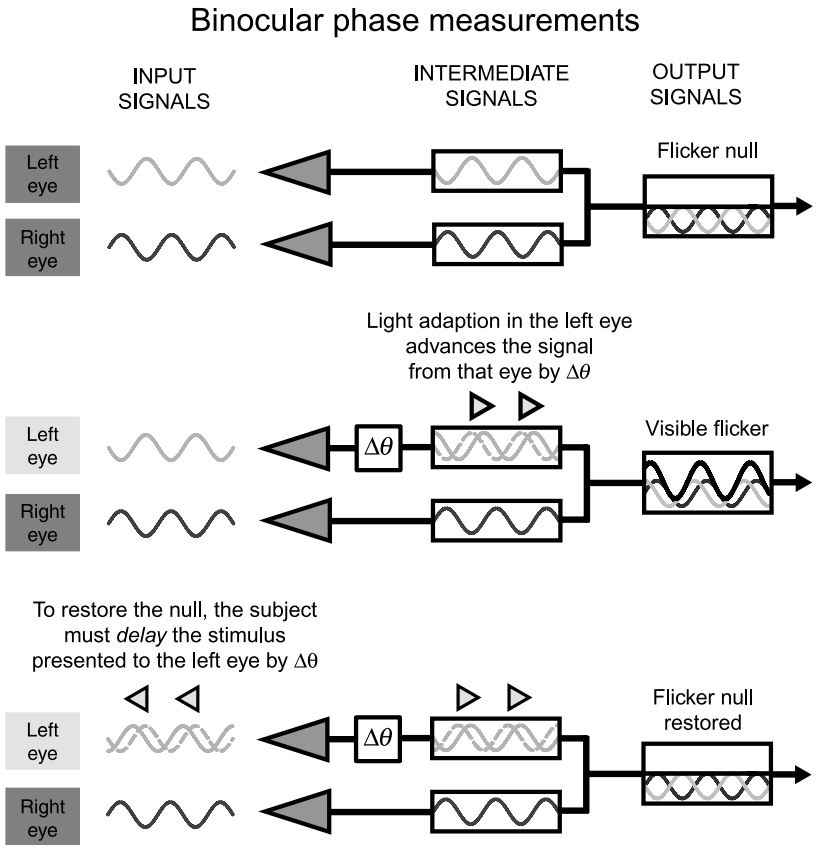

Figure 2. Illustration of the technique used to measure phase delays between stimuli seen by the left and right eyes. Flickering lights are presented separately to the left and right eyes (INPUT SIGNALS), which generate neural signals in response to the flicker (INTERMEDIATE SIGNALS). These signals are transmitted to the cortex, where the neural signals from the two eyes are combined (OUTPUT SIGNALS). Left eye signals are shown in light gray, right eye signals in dark gray, and the combined signals in the rightmost panels in black. The top panels show the left and right eyes under the same state of light adaptation. Thus, any adaptation-dependent phase delays should be the same so that opposite phase signals at the input will remain in opposite phase until they destructively interfere at the output, producing a flicker null (rightmost panel). In the middle and bottom panels, the left eye is more light adapted than the right eye, with the result that the left eye signal is phase advanced by $\Delta\theta$ relative to the right eye signal ($\Delta\theta$ equals 90° or 1/4 cycle in this example). Now, opposite phase signals at the input (middle panels) no longer null each other at the output. To restore the null (bottom panels), the signal seen by the left eye must be phase delayed by $\Delta\theta$ to compensate for the internal phase advance. The required adjustment provides an estimate of the interocular delay.

M-cone modulation thresholds

Figure 3 shows the logarithm of the M-cone temporal modulation threshold curves for M.L. (upper panel) and M.M. (lower panel) as a function of frequency (in hertz). Except at the lowest levels (see also Figure 4), the curves are bandpass in shape (i.e., they peak in sensitivity at an intermediate frequency). Although there are some differences between the overall shapes of the curves for M.M. and M.L., the *changes* in sensitivity between different levels of adaptation—which are what we actually model—are very similar (see Figure 6, upper panels). We speculate that the shape differences occur because M.M. has access to a residual low-frequency chromatic signal, arising from slight spectral sensitivity differences in his two expressed X-linked photopigments.

The data for both subjects can be usefully separated into two regions. In the first region, below 4.16 log td (denoted by the open symbols), high-frequency sensitivity increases with intensity more than low-frequency sensitivity, so that the functions become broader and extend to higher frequencies. In the second region, above 4.16 log td (denoted by the filled symbols), the shapes of the curves stay roughly constant. If the modulation thresholds are constant, Weber's law ($\Delta I/I = k$) holds, and the proportional sensitivity to superimposed lights is maintained as the luminance level is changed. This occurs mainly at low frequencies and at high intensities.

Another helpful way of visualizing the modulation threshold data is to plot the logarithm of the threshold amplitudes ($I_{max} - I_{min}$) as a function of frequency, as shown in Figure 4 for M.L. (left panel) and M.M. (right panel). This way of plotting the data emphasizes those

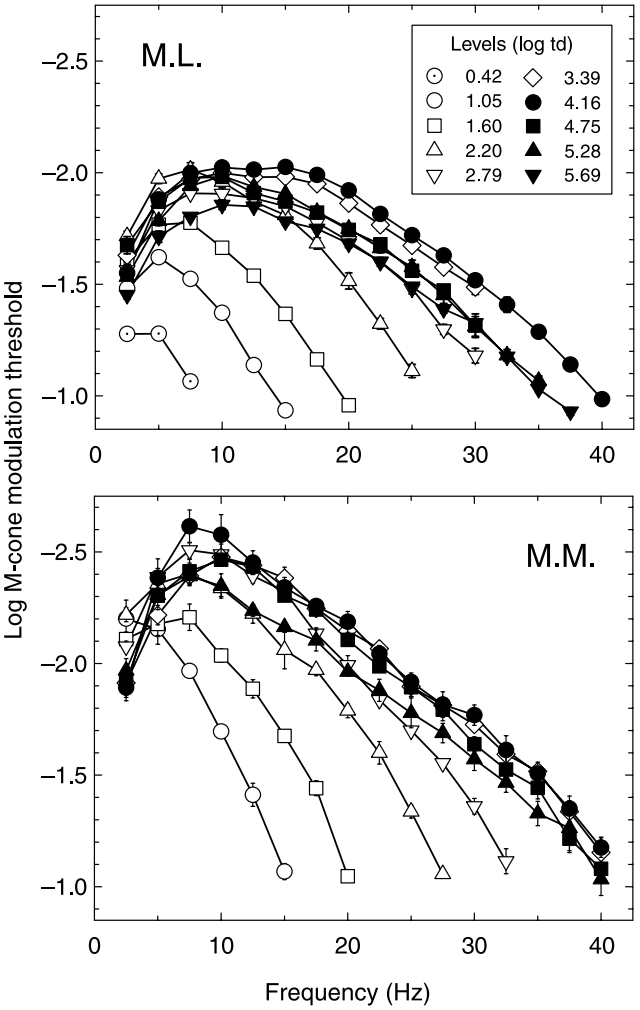

Figure 3. Logarithmic M-cone modulation thresholds for subjects M.L. (top panel) and M.M. (bottom panel) plotted against linear frequency. The adaptation level was varied according to the key. The lowest and highest levels were presented only to M.L.

levels between which the change in background has no effect on the amplitude required for detection (i.e., when $\Delta I = k$). Given some extrapolation to frequencies above the measurable range, such behavior, which is known as "high-frequency linearity," is found to occur between 0.42 and 2.79 log td for M.L. and to occur between 1.05 and 3.39 log td for M.M. Comparable data have been reported before (e.g., De Lange, 1958; Kelly, 1972; Roufs, 1972a).

The term "high-frequency linearity" was first used by Kelly (1961b) to describe his and De Lange's (1958) temporal modulation-sensitivity data, which indicated that the amplitude sensitivity for high temporal frequencies was roughly independent of the mean luminance level over a sizable range of luminances and frequencies. Kelly interpreted this independence as evidence that the visual system was behaving linearly under these conditions (i.e., it has a linear input–output function for high-frequency flicker, which is unaffected by adaptation). Such high-frequency linearity is also suggested, at least near threshold, by obedience to the Talbot–Plateau law, the well-known observation that lights flickering faster than the temporal acuity limit appear identical to lights of the same time-averaged radiance (Plateau, 1835; Talbot, 1834), and by the finding that the detection of complex high-frequency waveforms depends only on the first harmonic component (e.g., De Lange, 1954; Kelly, 1961a, 1964). High-frequency linearity implies that the flicker signal at higher frequencies is largely unaffected by adaptation. It therefore puts severe constraints on any model of adaptation because it rules out frequency-independent sensitivity scaling, as would result from the molecular mechanisms in Categories B and C. However, other interpretations of "high-frequency linearity" allow for adaptational nonlinearities. Graham and Hood (1992, p. 1382), for example, allow changes in integration time and changes in overall gain to combine to keep the high-frequency thresholds constant with adaptation. Whether or not the high-frequency flicker signal is modified by adaptation can be better addressed by combining the usual amplitude measurements with phase measurements because the phase data can disambiguate changes in integration time, which typically affect phase, from changes in overall gain, which do not. Although the amplitude data in Figure 4 *appear* to be consistent with high-frequency linearity, the phase data suggest that linearity fails (see below).

M-cone phase lags

Phase lags were measured using an extension of flicker photometry, in which the subject varied the relative phase as well as the modulation of two binocularly fused targets to abolish or minimize the subjective flicker (see the Methods section for details). Figure 5 shows the *relative* phase delays in degrees between M-cone flicker presented to the left and right eyes of M.L. (upper panel) and M.M. (lower panel). For each subject, the luminance level in the right eye was fixed at 4.16 log td, whereas that in the left was varied (see key). A phase delay of 0° implies that the phase delays in the left and right eyes are the same (or a factor of 360° different). Overall, the phase delays for M.M. and M.L. are very similar. In general, increasing the adaptation level in the left eye advances the flicker signal, whereas decreasing the adaptation level delays it. For both subjects, the responses in the left eye are delayed at levels below 4.16 log td because the eye is *less* light adapted than the right eye, whereas they are slightly advanced above 4.16 log td because the left eye is *more* light adapted.

The phase delays extend to only about 20 Hz, although the flicker itself can be seen up to 40 Hz. Above 20 Hz, the effects of binocular flicker cancellation are too small to enable phase settings to be made. Presumably, this limit is due, in part, to filtering before the site of binocular cancellation. In contrast, cancellation between different cone signals in the same eye is possible up to and

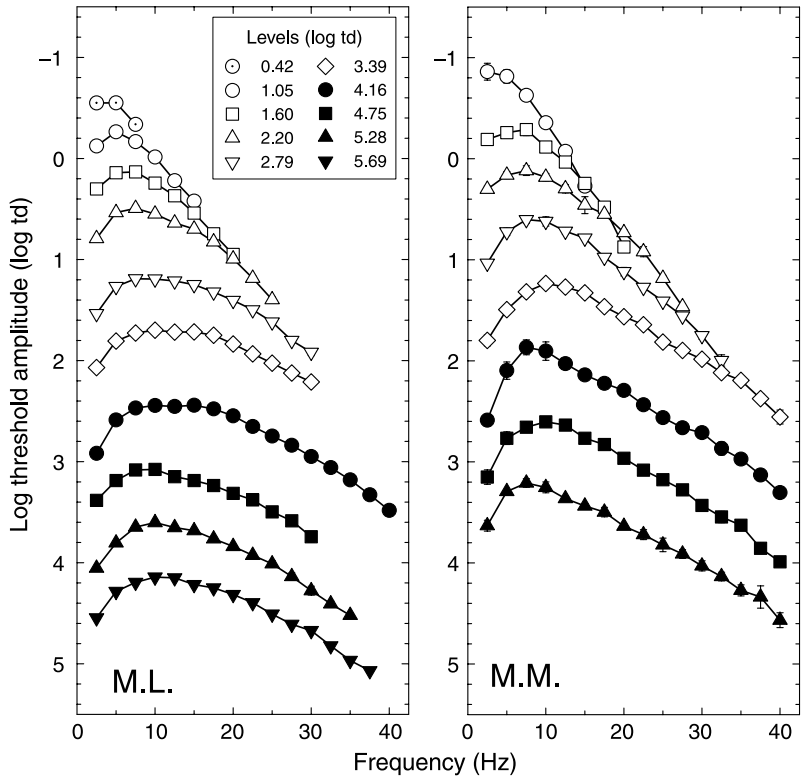

Figure 4. Data from Figure 3 plotted as logarithmic M-cone threshold amplitudes for subject M.L. (left panel) and M.M. (right panel).

sometimes well beyond the temporal acuity limit (e.g., Stockman, MacLeod, & Lebrun, 1993).

Like the sensitivity data, the phase data for both subjects can also be usefully separated into two regions. In the first region, below about 4.16 log td, the phase delays decrease as the adaptation level increases. In the second, at levels above 4.16 log td, the changes in phase delay are small. Control experiments carried out on M.L. using a 2.20 log td standard in the right eye rather than 4.16 log td confirm that this transition is independent of the standard used, as would be expected from the modulation-sensitivity changes.

Comparisons between Figures 4 and 5 show that large frequency-dependent changes in the shape of the amplitude (or modulation) sensitivity functions between levels are generally accompanied by large frequency-dependent changes in phase delay (open symbols). In contrast, frequency-independent changes (i.e., vertical shifts in the threshold amplitude functions with little or no changes in shape) are accompanied by little or no change in phase delay (closed symbols).

If adaptation does not modify the high-frequency flicker signal (in accordance with high-frequency linearity), then the convergence of the threshold amplitude data seen in Figure 4 should be accompanied by the changes in phase delay between levels falling back toward (and eventually reaching) zero. There is, however, no clear evidence for such a fallback in the phase-delay data with increasing frequency seen in Figure 5. This is partly because the phase data are limited to frequencies below 20 Hz, but it also suggests a failure of high-frequency linearity (see below).

Our phase-delay results are inconsistent with interocular phase measurements by Cavonius and Estévez (1980), who found that changes in luminance resulted in changes in phase delay of 48° per log unit that were *independent* of frequency (so that curves analogous to those in our Figure 5 would all be parallel). We suspect that their results, particularly those obtained at low frequencies, reflect the distortion of suprathreshold sinusoidal flicker producing unwanted signal components at higher frequencies. Unfortunately, however, very few methodological details were provided in their article. Intriguingly, though, some years later, Cavonius, Estévez, and van der Tweel (1992) reported that their counterphase dichoptic flicker produced visible second harmonic flicker.

Light adaptation models

Having both phase-delay and amplitude data allows us to better constrain and test models of human light adaptation than has been previously possible because any candidate model must simultaneously describe both types of data. Our goal, however, was not to find a complex, multiparameter, best fitting model but to find a simple, mainly *qualitative* model of adaptation that requires one or two intensity-dependent parameters. In light of the clear differences between the data measured in the regions above and

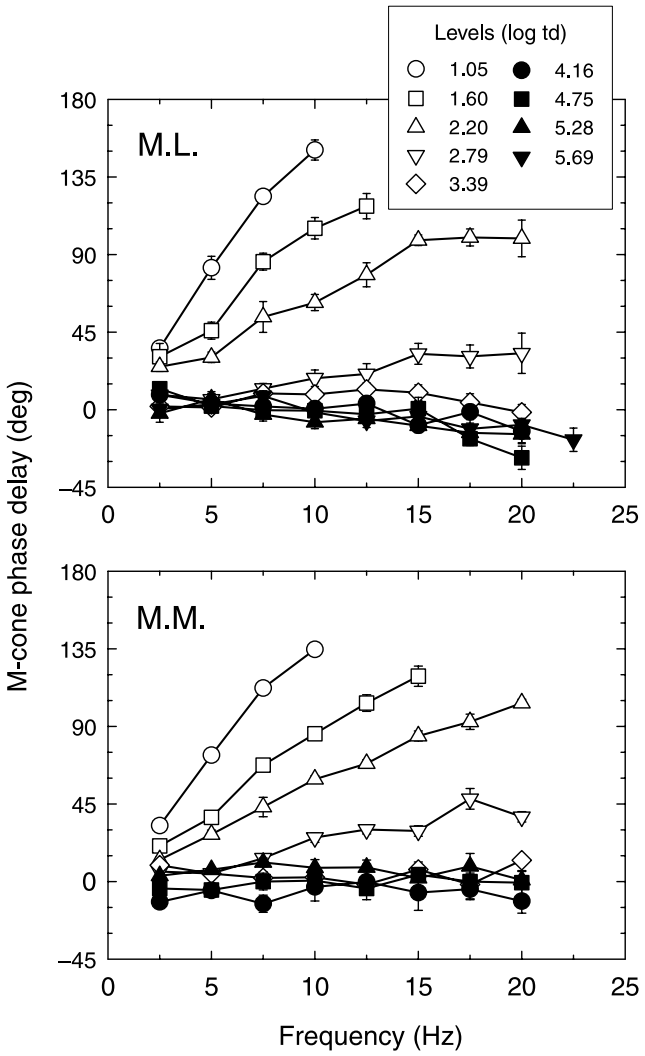

Figure 5. M-cone phase delays in degrees of signals generated in the left eye relative to those generated in the right eye for M.L. (top panel) and M.M. (bottom panel). The adaptation level in the right eye was fixed at 4.16 log td; that in the left eye was varied according to the key.

below 4.16 log td, we treated data from those two regions separately. Below circa 4.16 log photopic td, the amplitude and phase-delay data for both subjects show frequency-dependent changes, which are broadly consistent with a speeding up of the visual response and a shortening of the visual integration time. Above 4.16 log photopic td, adaptational changes are consistent with multiplicative scaling of the amplitude thresholds, as would be produced by bleaching. (In this region, the estimated time constants are in any case too short for adaptational changes to have a significant effect on the shapes of the amplitude and phase data in the visible range of frequencies.)

Adaptation below bleaching levels

For data obtained below circa 4.16 log photopic td, we first took the well-known and by now classic approach of modeling frequency-dependent changes in amplitude and phase by shortening the time constants (τ) of one or more (n) cascaded leaky integrating stages (or buffered RC circuits), which we also refer to as filters (see Watson, 1986). This approach (see the Discussion section), which was first proposed long before the details of the phototransduction cascade were understood, is still relevant in the context of cascade processes because leaky integrators are comparable to first-order biochemical reactions. In the filter, the response to a pulse decays exponentially with time, whereas in the reaction, the concentration of the reactant decays exponentially with time. The formula for the amplitude response, $A(f)$, of n cascaded leaky integrators is

$$A(f) = \tau^n \left[(2\pi f\tau)^2 + 1\right]^{\frac{-n}{2}}, \quad (1)$$

and the formula for the phase response, $P(f)$, is

$$P(f) = n \tan^{-1}(2\pi f\tau), \quad (2)$$

where f is the frequency in cycles per second (hertz) and τ is the time constant in seconds. There are two important properties of the cascade, which can be inferred from consideration of Equations 1 and 2. First, when the frequency f is high relative to $1/(2\pi\tau)$ (the so-called cutoff or corner frequency of a low-pass filter in hertz), the amplitude and phase are effectively *independent* of changes in the time constant, because in the case of $A(f)$, $A(f) \approx (2\pi f)^{-n}$, and then in the case of $P(f)$, $P(f) = n \times 90°$. Thus, a cascade can obey "high-frequency linearity." Second, when the frequency is low, the loss of sensitivity is proportional to the shortening of the time constant raised to the power of the number of integrators. Thus, a cascade that obeys high-frequency linearity can also, in principle, obey Weber's law, given the appropriate intensity-dependent changes in τ.

Our phase-delay measurements are, of course, relative data. We have no direct knowledge of the *absolute* phase delays of the visual system under these conditions. We therefore restrict our modeling to account for the *changes* in phase delay and the *changes* in log threshold amplitude between the six successive levels from 1.60 to 4.16 log td, which are shown in Figure 6 for M.L. (left panels) and M.M. (right panels).

In optimizing the two model parameters n (which we assume is independent of intensity) and τ (which is intensity dependent), the time constants of each of the n filters were varied together, thus altering the threshold amplitudes according to Equation 1 and the phase delays according to Equation 2. Allowing the time constants of each filter to vary independently yielded extra parameters but did not significantly improve the predictions of the model. We therefore yoked the time constants together, but we recognize that, in reality, the time constants of different stages are unlikely to be identical. The phase and amplitude

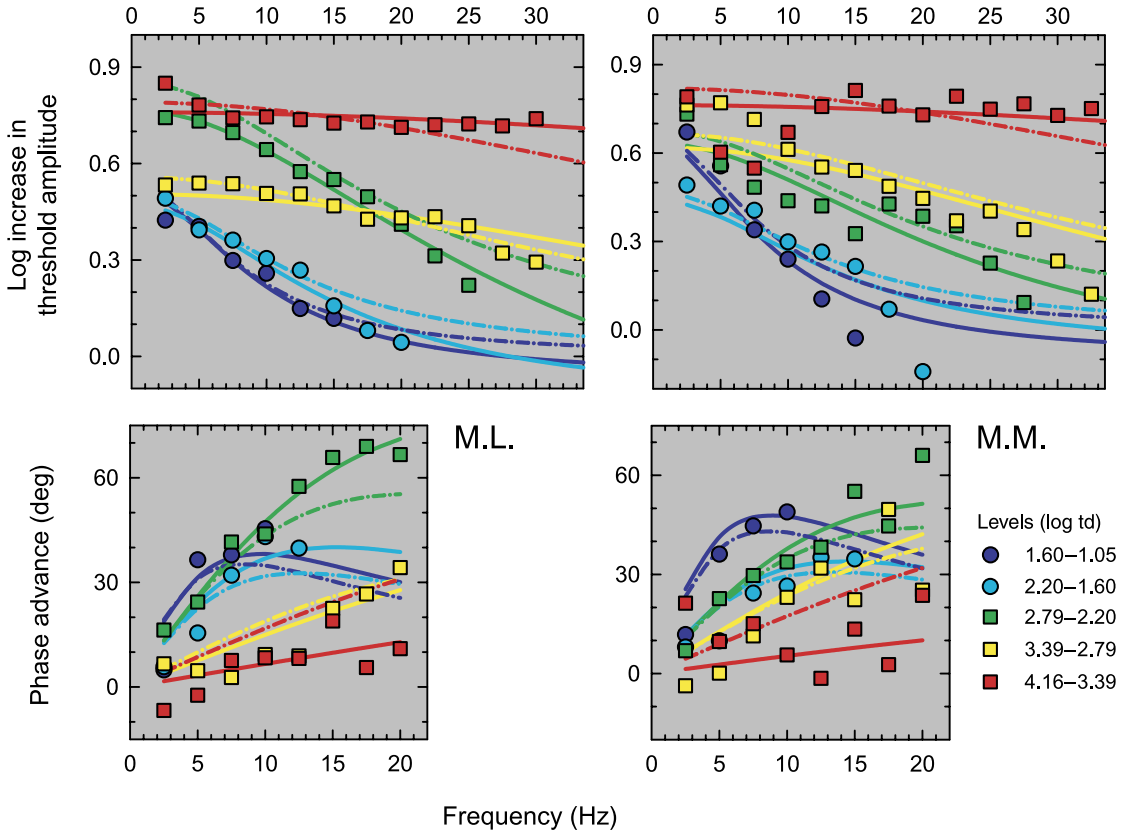

Figure 6. Adaptation below bleaching levels. Simultaneous fits of Model 1 (time constant only; dotted-dashed lines) and Model 2 (time constant and scaling; continuous lines) to the amplitude differences (symbols, upper panels) and phase-delay differences (symbols, lower panels) between successive levels for M.L. (left panels) and M.M. (right panels). The levels are noted in the key; the same color code is used for the symbols and for the model predictions.

data were weighted so that their influence was approximately equal (otherwise, one or other sets of data would dominate). When n was allowed to take on noninteger values, the best fitting models for both subjects lay between $n = 2$ and $n = 3$. We have chosen to show model predictions for $n = 3$ because $n = 3$ is also consistent with the subsequent model in which sensitivity scaling is also allowed. We emphasize, however, that n is poorly constrained by the fit because increases in n can be offset by decreases in τ and vice versa. The data, however, require that $n \geq 2$ because the phase changes with adaptation are greater than 90°, the maximum change for one filter. The model fits for $n = 3$ are shown by the dotted-dashed lines, which are color coded in the same way as the symbols. We refer to this as "Model 1: time constant only" because the only intensity-dependent parameter is τ.

As can be seen, Model 1 does a reasonably good job of accounting for the changes in amplitude thresholds with adaptation. Relative to the null model that there is no change in amplitude or phase between levels (i.e., all the values in Figure 6 are zero), the single-parameter model accounts for 99.17% of the variance in threshold amplitude and 90.75% of the variance in phase for M.L. and 96.28% of the threshold amplitude and 87.50% of the phase variance for M.M. Relative to the mean of each data set, the single-parameter model accounts for 94.68% of the threshold amplitude and 77.86% of the phase variance for M.L. and 79.98% of the threshold amplitude and 63.20% of the phase variance for M.M. In general, the model predictions are better for M.L. than for M.M., and the amplitude predictions are better than the phase predictions. Given that this model has just a *single* intensity-dependent parameter, τ, the predictions are, we believe, impressive. Although this single intensity-dependent parameter model predicts the data moderately well, there are some discrepancies. We next tried to reduce them by extending the model.

Many modifications to the model of varying complexity are possible. To keep it simple, we chose to add only a single, extra intensity-dependent parameter. A biologically plausible adjustment in terms of the molecular mechanisms described above is to allow a frequency-independent "turning up or down" of the visual response by multiplicatively scaling the amplitude thresholds (i.e., by shifting the logarithmic functions threshold amplitude functions vertically without changing their shape) while leaving the phase delays unaffected (i.e., mechanisms in Categories B and C, above). The two intensity-dependent

parameter model fits are shown by the continuous lines in Figure 6, which are again color coded in the same way as the symbols. We refer to this as "Model 2: time constant and scaling." The predictions are clearly better than for Model 1. Relative to the null model that there is no change in amplitude or phase between levels, the two-parameter model accounts for 99.64% of the threshold amplitude and 97.07% of the phase variance for M.L. and 97.55% of the threshold amplitude and 91.18% of the phase variance for M.M. Relative to the mean of each set of data, the two-parameter model accounts for 97.73% of the threshold amplitude and 92.98% of the phase variance for M.L. and 86.85% of the threshold amplitude and 74.03% of the phase variance for M.M. More complex models with more parameters would, of course, further improve the predictions, but when we tried various alternatives, the improvements were small.

The time constants (diamonds) assumed in Model 2, the time-constant-and-scaling model, are shown in the upper panels of Figure 7 for M.L. (left) and M.M. (right). For

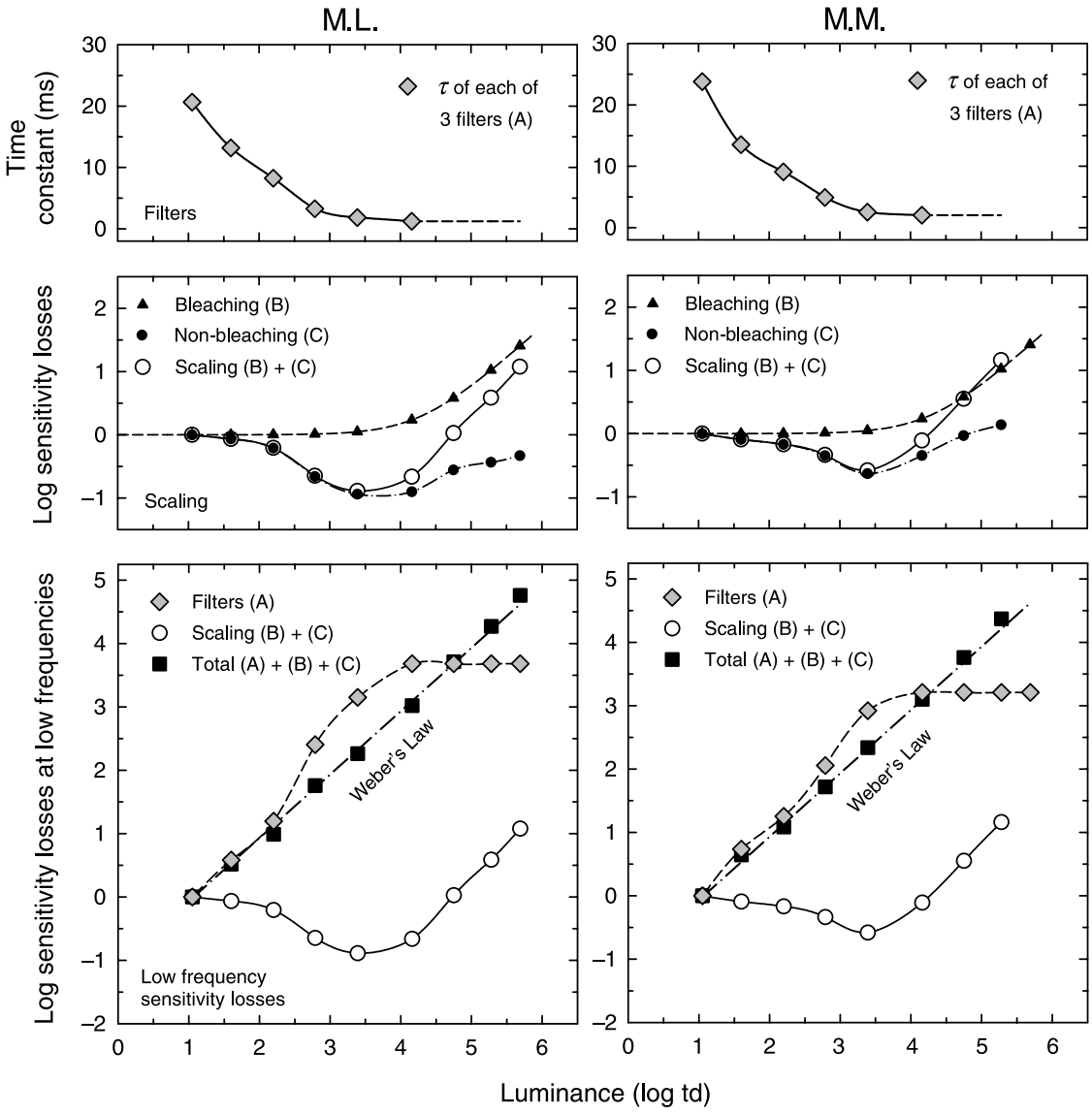

Figure 7. Parameters for Model 2, the time-constant-and-scaling model, for M.L. (left panels) and M.M. (right panels). Upper panels: dependence of the time constant of each of the three integrating stages on luminance (A, gray diamonds). The time constants are assumed to remain constant above 4.16 log td (dashed line). Middle panels: cumulative logarithmic sensitivity losses assumed to be caused by multiplicative scaling (B + C, open circles), subdivided into the losses calculated to be caused by photopigment depletion (B, filled diamonds) and by other factors (C, filled circles). Lower panels: cumulative logarithmic sensitivity losses at low frequencies due to shortening time constants (A, gray diamonds) and sensitivity scaling (B + C, open circles, replotted from middle panels). The combined low-frequency losses (A + B + C, filled squares) agree with Weber's law (dotted-dashed lines). For the derivation of the parameters at luminances below 4.16 log td, see the Adaptation below bleaching levels section, and for derivation of the parameters at luminances above 4.16 log td, see the Adaptation at bleaching levels section.

both subjects, the constants shorten rapidly between 1.06 and 2.79 log td but then more slowly between 2.79 and 4.16 log td. Above 4.16 log td, they are assumed to be constant (see below). A logarithmic plot of the dependence of the time constant on luminance is shown as the filled diamonds in Figure 9. The *cumulative* sensitivity scaling assumed in Model 2 is shown in the middle panel of Figure 7 by the open circles (for details above 4.16 log td, see the next section). Importantly, the scaling *improves* sensitivity between 1.05 and 2.79 log td for M.L. or between 1.05 and 3.39 log td for M.M. (see Figure 7). The sensitivity improvements are by factors of more than 8 and 4 for M.L. and M.M., respectively. Again, we emphasize that n is poorly constrained. The predicted time constants for versions of Model 2 with $n = 2$, 3, and 4 are compared in Figure 9 (see the Discussion section).

Adaptation at bleaching levels

Using standard steady-state bleaching equations, we calculate that levels of 3.39, 4.16, 4.75, 5.28, and 5.69 log td bleach approximately 11%, 42%, 74%, 91%, and 96% of the pigment, respectively, assuming a half-bleaching constant (I_0) of 4.30 log td and the fraction of unbleached pigment, $p = I/(I + I_0)$ (Rushton, 1963, 1965). Thus, the effect of bleaching on sensitivity starts to become significant above circa 4.16 log photopic td. Accordingly, we modeled the sensitivity losses between those levels as a multiplicative scaling of the amplitude thresholds (i.e., as vertical shifts of the logarithmic threshold amplitude functions without change of shape), which is consistent with the effects of photopigment depletion. To estimate the logarithmic shifts, we used two related methods, which gave results within 0.01 $\log_{10}$ unit of each other. Using a least squares fitting criterion, the data from 4.75 to 5.69 log td were shifted to vertically align with the data for 4.16 log td. The aligned data were then either (i) averaged to produce a mean function or (ii) entered into a curve generation program to produce an arbitrary mean template shape. Thereafter, the individual data were vertically shifted to fit either the mean function or the mean template. Carrying out these procedures iteratively did not significantly change the fits. The calculated shifts, plotted cumulatively, are shown as the open circles in the middle panels of Figure 7 (above 4.16 log td).

Discussion

The novel combination of amplitude and phase measurements reported here constrains models of light adaptation better than has been possible with psychophysical data before. Most of the variance can be accounted for by Model 2, which has two intensity-dependent factors: shortening time constants and sensitivity scaling. Figure 8 shows the final form of the model. The first intensity-dependent parameter of the model, following the cones on the left of the figure, is the time constant of a cascade of n leaky integrators (A), which, *for simplicity,* are assumed to shorten together with adaptation (gray diamonds, Figure 7) but, in reality, are unlikely to be yoked together. The second intensity-dependent parameter is multiplicative sensitivity scaling (open circles, Figure 7), which we have subdivided into sensitivity scaling that reduces sensitivity (B) and sensitivity scaling that increases sensitivity (C). Sensitivity scaling that reduces sensitivity has been further subdivided into photopigment depletion or bleaching (B_1), response compression (B_2), and other neural factors (B_3). We show sensitivity scaling due to response compression as a separate element in the model (B_2) for completeness. However, its effects, if any, cannot be distinguished from those of other factors (B_3).

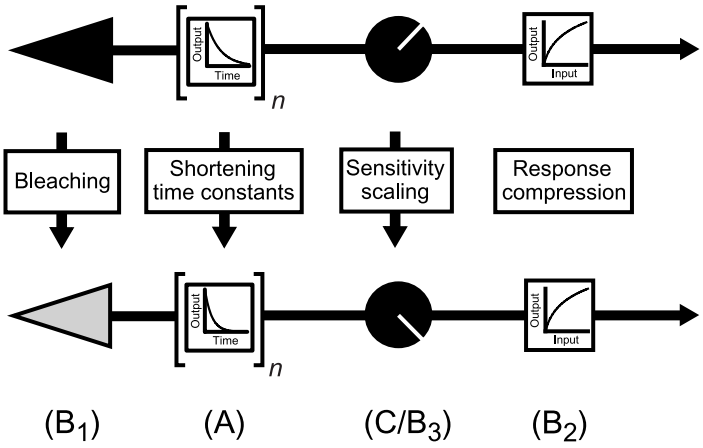

Figure 8. The final model made up of n leaky integrators (A), the time constants of which shorten together with adaptation, and sensitivity scaling. Sensitivity scaling is assumed to either increase sensitivity (C) or to decrease sensitivity (B). Sensitivity scaling that decreases sensitivity can be photopigment bleaching (B_1), response compression (B_2), or other factors (B_3).

Each stage of the model can be loosely linked to the molecular processes occurring within the photoreceptor that we categorized in the Introduction section. The shortening time constants of the filters can be linked to (i) the increase in the rate of cGMP hydrolysis mediated by the light-induced rise in the concentration of PDE6* and (ii) the decrease in the lifetime of R* mediated by RK mechanisms (from Category A). The number of filters (n) is poorly constrained by the model fits. Although we chose to use three filters in our model, we could have chosen between two and four filters with proportionally shorter time constants for fewer filters. The trade-off between filters and time constants is discussed in the next section. The remaining components of the model can be linked to (i) pigment bleaching and (ii) response compression (from Category B), which decrease sensitivity, and to (i) the increase in the rate of cGMP synthesis and (ii) the decrease in sensitivity of the CNG channels (from Category C), which increase sensitivity. Given, however, that the model just provides an estimate of the *overall* scaling, we can only estimate the effects of each of these different underlying mechanisms.

The most straightforward scaling "mechanism" is photopigment bleaching, which reduces the number of available photopigment molecules. As noted above, the levels of 4.16, 4.75, 5.28, and 5.69 log td bleach approximately 42%, 74%, 91%, and 96% of the pigment, respectively. The expected cumulative sensitivity losses due to such photopigment depletion are shown by the triangles in the middle panels of Figure 7. The remaining sensitivity losses, which must be due to other scaling mechanisms (i.e., the differences between the open circles and triangles), are shown by the filled circles. The losses above 4.16 log td *in addition to* photopigment depletion could be due to bleaching desensitization, the additional loss of sensitivity caused by bleaching photoproducts (see Fain, Matthews, & Cornwall, 1996; Fain et al., 2001; Lamb & Pugh, 2004; Leibrock, Reuter, & Lamb, 1998; Pepperberg, 2003), to pigment depletion being higher than predicted by standard equations (e.g., Burns & Elsner, 1985, 1989; Mahroo & Lamb, 2004; Reeves, Wu, & Schirillo, 1998; Smith, Pokorny, & van Norren, 1983), or to other factors.

Perhaps the most interesting aspect of the model is that sensitivity scaling causes an increase in sensitivity below 4.16 log td. As can be seen in Figure 7, this reaches a cumulative gain in sensitivity of circa 0.9 log unit for M.L. (a factor of 8) and circa 0.6 log unit for M.M. (a factor of 4). Although consistent with the molecular models of adaptation, this increase is inconsistent with the conventional psychophysical view of adaptation (see the Relationship to previous models section). We link these effects to (i) the increase in the rate of cGMP synthesis and (ii) the decrease in sensitivity of the CNG channels from Category C. We note that the combined sensitivity gains due to these two molecular factors could be larger than the model predictions because the measured gains could be reduced by losses due to other mechanisms (in Category B).

The last component in the model, which we show separately, is a nonlinearity that gives rise to response compression (B_2). We link this to response compression from Category B caused by a reduction in open CNG channels. We speculate that this mechanism may play only a small role in our experiments because they were carried out under steady-state conditions using near-threshold flickering targets. Response compression would presumably play a much greater role if the illumination changes were large and rapid.

In general, we find no evidence for a change in the numbers of integrators with adaptation. We also find no clear evidence for high-pass filtering stages that change their time constants or weights with adaptation—the increasingly bandpass nature of the temporal frequency response in our data can be accounted for solely by shortening time constants.

Time constants and the number of filters

It is difficult to determine unequivocally the number of filters (n) and the time constant of each filter (τ) because the two parameters interact in the model fits: An increase in one parameter can partially offset a decrease in the other. We can explore the relationship between the two by fitting versions of Model 2, the time-constant-and-scaling model, with different values of n to the amplitude and phase data. Figure 9 shows the best fitting values of τ for $n = 2$ (open inverted triangles), $n = 3$ (filled diamonds), and $n = 4$ (open triangles) filters for M.L. (upper panel) and M.M. (lower panel) plotted in double-logarithmic coordinates. It is immediately apparent that, for each set of predictions, the relationship between $\log(\tau)$ and log luminance, which we refer to as $\log(I)$, is approximately linear. Least squares linear regression provides the following estimates of the slopes: -0.68, -0.46, and -0.34 for $n = 2$, 3, and 4, respectively, for M.L. and -0.60, -0.41, and -0.30 for M.M. Thus, the mean slopes across n are $-1.37/n$ for M.L. and $-1.21/n$ for M.M. These slopes provide an approximate *general* solution for how yoked time constants shorten with light adaptation for different n values.

Were the number of filters and reductions in time constants tuned for Weber's law, the slopes in Figure 9 would be -0.5, -0.33, and -0.25 for $n = 2$, 3, and 4, respectively, and $A(0) \propto I^{-1}$ (i.e., the amplitude of the steady component at 0 Hz would be inversely proportional to the mean luminance and, therefore, constant). Because Weber's law does hold (see Figure 7), the *increases* in sensitivity caused by scaling must therefore approximate to $A(0) \propto I^{0.36}$ for M.L. and $A(0) \propto I^{0.20}$ for M.M. to compensate for the losses in excess of Weber's law caused by the shortening time constants. Given that Weber's law holds so precisely, despite differences in time constants between observers, there must presumably be some

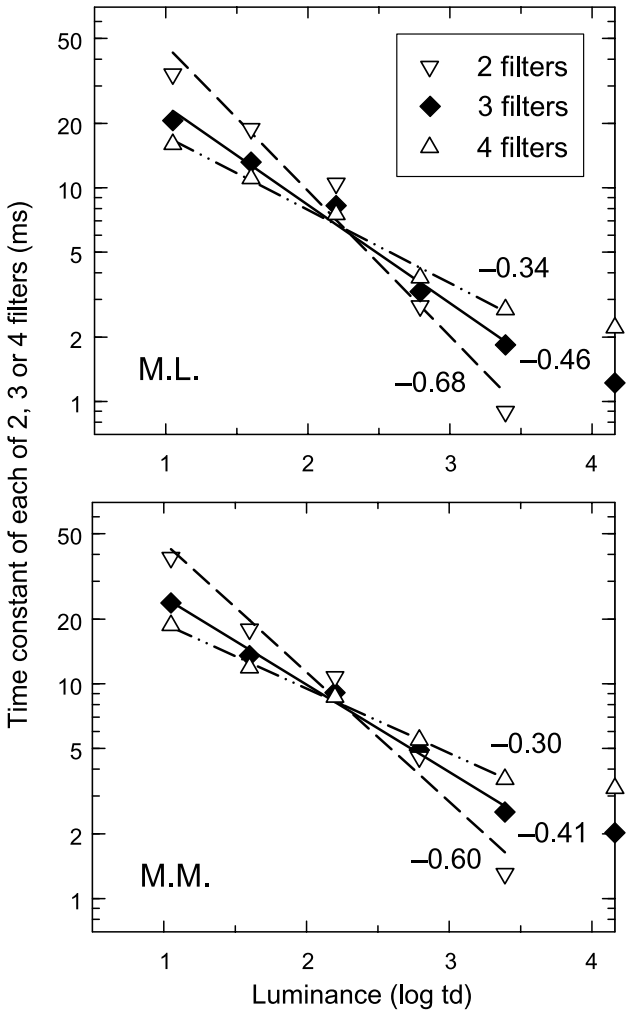

Figure 9. Time constants for each filter in milliseconds for versions of Model 2 with two (open inverted triangles), three (filled diamonds), or four (open triangles) filters for M.L. (upper panel) and M.M. (lower panel). Each function can be approximated by a straight line in double-logarithmic coordinates, the best fitting versions of which are shown by the dashed (two filters), solid (three filters), and dotted-dashed (four filters) lines. The slopes of the best fitting lines are noted in the figure. The previously shown fits and model parameters shown in earlier figures correspond to the three-filter version of the model (see above).

control system that compensates for the losses in excess of Weber's law and restores it.

Site of adaptation

We have linked our model to molecular mechanisms of adaptation occurring within the photoreceptor. However, psychophysical measurements inevitably involve many more neural stages than just the photoreceptors. Nevertheless, we suspect that for our experimental conditions, postreceptoral mechanisms play only a small role. Granted some evidence has suggested that little adaptation occurs within photoreceptors until close to bleaching levels (e.g., Hood & Birch, 1993; Schnapf, Nunn, Meister, & Baylor, 1990), but other compelling evidence suggests that significant adaptation occurs at much lower light levels (e.g., Boynton & Whitten, 1970; Burkhardt, 1994; Valeton & van Norren, 1983). Measures of adaptation in monkey horizontal cells show that light adaptation is well advanced at or before the first synapse in the visual pathway and begins at levels as low as 15 td (Lee, Dacey, Smith, & Pokorny, 1999, 2003), which corresponds to the lower end of our range of measurements. Moreover, psychophysically, local adaptation has been demonstrated to occur with the resolution of single cones (Burton, 1973; MacLeod & He, 1993; MacLeod, Williams, & Makous, 1992). On balance, then, the available evidence supports a receptoral site of cone adaptation.

Reconstructions of the amplitude thresholds and phase delays

Although the fits shown in Figure 6 summarize the model predictions, it is instructive to use them to reconstruct the original data. Such reconstructions are shown in Figure 10 for M.L. and in Figure 11 for M.M. The reconstructions were achieved in three steps. First, Model 2, the time-constant-and-scaling model, was used to adjust each set of phase and amplitude data back to the *same* level of 2.79 log td (e.g., the 1.60 log td data were adjusted to 2.79 log td using the predicted differences between 1.60 and 2.20 log td *and* between 2.20 and 2.79 log td; the 2.20 log td data were adjusted to 2.79 log td using the predicted differences between 2.20 and 2.79 log td, etc.). Second, a mean smoothed template was derived for each subject to describe all his amplitude data adjusted to 2.79 log td and then another template was derived to describe all his phase data adjusted to 2.79 log td. The templates were derived using a curve discovery program (TableCurve 2D, Jandel Scientific). They are the smooth functions fitted to the 2.79 log td data in Figures 10 and 11, the formulae for which are provided in the Appendix. Finally, the model predictions were used to adjust the smoothed templates for 2.79 log td back to each of the intensity levels (e.g., the smoothed 2.79 log td template was adjusted to 1.60 log td using the predicted differences between 1.60 and 2.20 log td *and* between 2.20 and 2.79 log td, etc.). Above 4.16 log td, only scaling is assumed in the model; thus, in this range, the amplitude template is fixed in shape and vertically shifted. The templates adjusted for each level are shown in Figures 10 and 11 as the continuous lines (we attach no special significance to formulae for the template functions).

The errors in the reconstruction are cumulative; hence, they should worsen as the level is decreased or increased away from 2.79 log td. Nevertheless, despite some discrepancies, the templates describe the data remarkably well over the entire luminance range. One interesting

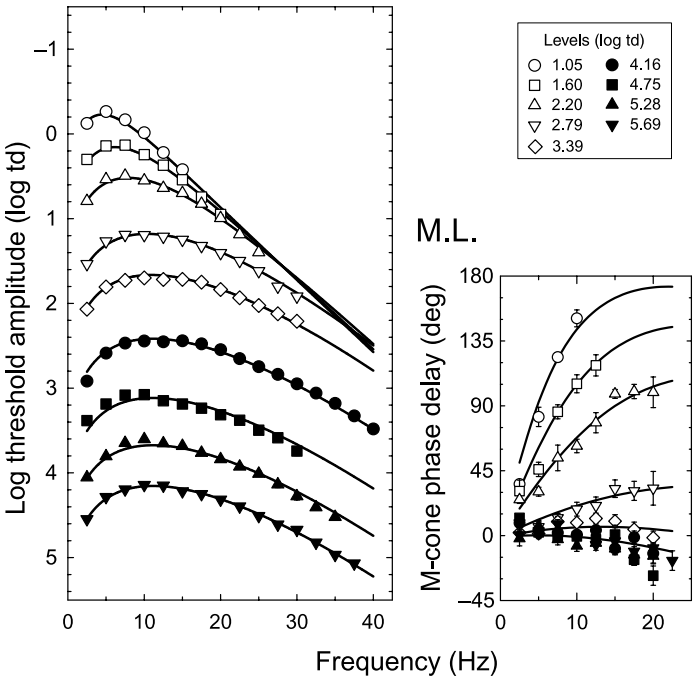

Figure 10. Logarithmic threshold amplitudes (symbols, left panels) and phase delays (symbols, right panels) for M.L. and predictions of Model 2 reconstructed according to details in the text (solid lines). The levels are noted in the key.

observation is that when both eyes are adapted to the same luminance level of 4.16 log td, the phase delays are not precisely zero. Indeed, our results, particularly those for M.L., show that one eye is effectively more light adapted than the other, although they are both exposed to the same luminance levels. This could be due to interocular differences in preretinal filtering or other factors, but it may suggest that the self-calibration mechanisms in each eye are relatively imprecise.

Features of the model

Weber's law holds at low frequencies

As illustrated in the lower panels of Figure 7, at low frequencies, the sensitivity losses caused by the shortening time constants (A, gray diamonds) combined with the sensitivity gains or losses caused by sensitivity scaling (B + C, open circles) together (A + B + C, filled squares) follow Weber's law (dotted-dashed line). Thus, Weber's law is maintained mainly by shortening time constants at the lowest levels, by the combined effects of the shortening time constants and sensitivity scaling at intermediate levels, and by sensitivity scaling at the highest levels.

Linearity fails at high frequencies

In the data, high-frequency linearity fails. This failure is clear at high adaptation levels, where bleaching—as expected—causes substantial frequency-independent sensitivity losses that result in the vertical separation of the amplitude threshold curves (filled symbols and predictions, Figures 10 and 11). Although less clear, high-frequency linearity also fails at lower levels but now because of frequency-independent sensitivity *gains*. These failures are much less conspicuous in the amplitude data because the sensitivity gains shift the amplitude threshold curves *together* so that they still seem to converge in the way required of high-frequency linearity. However, the convergence occurs at temporal frequencies too low to be consistent with the phase-delay data, which should themselves converge to zero (such a convergence is predicted by the model but at higher frequencies than we can measure).

Relationship to previous models

We acknowledge our debt to previous models of light adaptation, many of which incorporated some of the elements used in our model. Most previous models have tended to be specific to the type of data upon which they were based. Typically, those based on human temporal modulation threshold data have been designed to account for the principal features of such data: (1) the increasing sensitivity to higher temporal frequencies, (2) the increasingly bandpass nature of the response, (3) high-frequency linearity, and (4) Weber's law at low frequencies (see, e.g., De Lange, 1958, 1961; Kelly, 1961b; Matin, 1968;

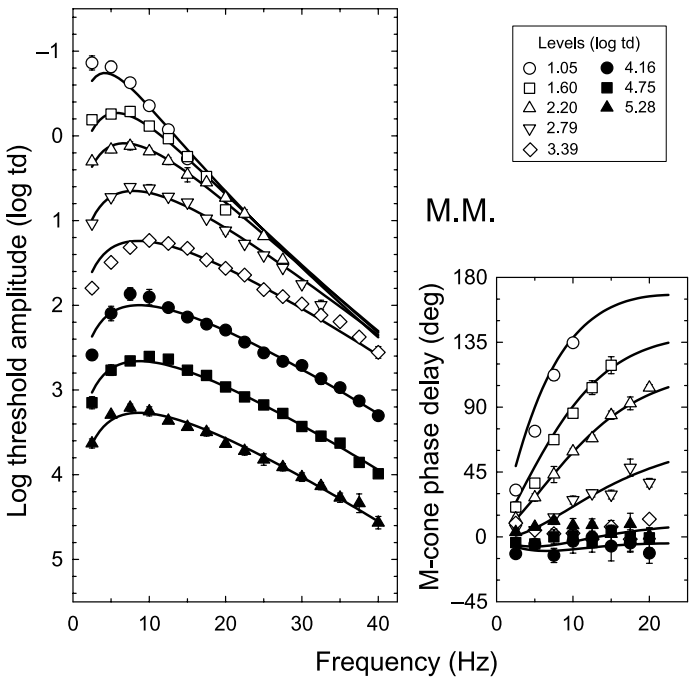

Figure 11. Logarithmic threshold amplitudes and phase delays for M.M. and predictions of Model 2. Details are the same as Figure 10.

Roufs, 1972b; Sperling & Sondhi, 1968; Tranchina, Gordon, & Shapley, 1984; Watson, 1986). Such models, like the one proposed here, include cascades of low-pass, leaky integrators, the time constants of some or all of which shorten with adaptation. In addition, many models incorporate high-pass stages or control the time constants of the low-pass filters with delayed feedback or feedforward to make the response increasingly bandpass with adaptation.

The combined modulation threshold and phase-delay data presented here provide a strong test of previous models based solely on temporal modulation threshold data. First, they suggest that high-frequency linearity fails. Of the human models, only the compromise models of Graham and Hood (1992), which were partly based on probe-flash data (see below) and thought therefore to be incompatible with temporal modulation threshold data, fail to show high-frequency linearity. Second, our data suggest that the increasingly bandpass nature of the frequency response is accomplished solely by shortening time constants, without the need for adaptational *changes* in high-pass filtering. Such a feature is found in the model of Kelly (1961b). Third, our data do not require a change in the number of integrators with adaptation.

Models based on photoreceptor responses to brief flashes of light are also guided by data that, in principle, contain both amplitude and phase information (e.g., Baylor & Hodgkin, 1974; Baylor et al., 1974; Fuortes & Hodgkin, 1964; Penn & Hagins, 1972). The model proposed here also has features in common with photoreceptor-based models, with the exception of the frequency-independent gains in sensitivity.

A distinct genre of adaptation models are those that account for the changes in sensitivity for a probe flash following an abrupt increase in background luminance (e.g., Geisler, 1978; Hayhoe, Benimoff, & Hood, 1987; Hood, Finkelstein, & Buckingham, 1979). A characteristic finding, known as the background-onset effect, is that the threshold for a probe coincident with background onset is higher than it is for delayed probes. In general, such models require an instantaneous static nonlinearity, which compresses the large coincident response and spares it from complete saturation, combined with delayed multiplicative scaling and subtractive adaptation (the discounting of the background) that together restore adaptation to its steady-state level. Given the requisite for a nonlinearity, such models have understandably ignored temporal frequency data, with which—if high-frequency linearity holds—they are inconsistent.

Our finding that high-frequency linearity does not hold in temporal frequency data may provide the necessary bridge between the background-onset models and the temporal-frequency-data models and support so-called merged or compromise models (Graham & Hood, 1992; Hood, Graham, von Wiegand, & Chase, 1997; von Wiegand, Hood, & Graham, 1995) that have previously tried to bridge the two classes. Our model, in fact, contains both the multiplicative stage and the nonlinearity found in background-onset models. An adaptation-independent subtractive stage is also implied by the bandpass nature of the underlying temporal frequency response that *does not change* with adaptation (lowest curves, left panels of Figures 10 and 11), which selectively attenuates steady signals generated by backgrounds.

A new class of molecular-based models is being developed to account for physiological and ERG data. The recent model of van Hateren (2005) combines low-pass filters, static nonlinearities, and feedback loops with a multiplicity of optimized model parameters to predict primate horizontal cell data (Lee et al., 2003; Smith, Pokorny, Lee, & Dacey, 2001). Although many features of the horizontal cell data are likely to be visually insignificant at the perceptual level (certainly when compared with steady-state flicker measurements), these new models should be consistent at some level with psychophysical data and models.

Conclusions

As the cone visual system light adapts over 5 log units of intensity, the accompanying changes in amplitude sensitivity and phase delay can be accounted for by a cascade of three leaky integrators, the time constants of which shorten with adaptation, and frequency-independent sensitivity scaling.

Appendix

The arbitrary template formulae for 2.79 log td used in Figures 10 and 11, where a is the amplitude threshold in log td, p is the phase delay in degrees, and f is the frequency in hertz, are as follows:
For subject M.L., the amplitude template is

$$\log(a) = 2.8920 + 0.1365f - 0.8783f^{0.5}$$

and the phase template is

$$p = -0.8893 + 2.6547f - 0.0498f^{2}.$$

For subject M.M., the amplitude template is

$$\log(a) = 3.9212 + 0.5279f^{0.5}\ln(f) - 2.1481f^{0.5}$$

and the phase template for 2.79 log td is

$$p = (-0.9818 + 0.2986f^{2})/(1 + 0.0038f^{2}).$$

Acknowledgments

This work was supported by a Wellcome Trust grant and by NIH Grant EY10206 both awarded to A.S. We thank Matt McMahon for services as a subject, Rhea Eskew and Donald MacLeod for helpful advice, Bruce Henning and Trevor Lamb for comments on the manuscript, and John Robson for the initial inspiration during a walk in Sarasota many years ago.

Commercial relationships: none.
Corresponding author: Andrew Stockman.
Email: a.stockman@ucl.ac.uk.
Address: Institute of Ophthalmology, University College London, 11–43 Bath Street, London EC1V 9EL, UK.

References

Arshavsky, V. Y., Lamb, T. D., & Pugh, E. N., Jr. (2002). G proteins and phototransduction. *Annual Review of Physiology, 64,* 153–187. [PubMed]

Baker, C. H. (1952a). The dependence of binocular fusion on timing of peripheral stimuli and on central process: 1. Symmetrical flicker. *Canadian Journal of Psychology, 6,* 1–10. [PubMed]

Baker, C. H. (1952b). The dependence of binocular fusion on timing of peripheral stimuli and on central process. *Canadian Journal of Psychology, 6,* 84–91. [PubMed]

Baker, C. H. (1952c). The dependence of binocular fusion on timing of peripheral stimuli and on central process: 2. Asymmetrical flicker. *Canadian Journal of Psychology, 6,* 123–130. [PubMed]

Baker, C. H. (1952d). The dependence of binocular fusion on timing of peripheral stimuli and on central process: 3. Cortical flicker. *Canadian Journal of Psychology, 6,* 151–163. [PubMed]

Baker, C. H., & Bott, E. A. (1951). Studies on visual flicker and fusion: II. Effects of timing of visual stimuli on binocular fusion and flicker. *Canadian Journal of Psychology, 5,* 9–17. [PubMed]

Barlow, H. B., & Levick, W. R. (1976). Threshold setting by the surround of cat retinal ganglion cells. *The Journal of Physiology, 259,* 737–757. [PubMed] [Article]

Bauer, P. J. (1996). Cyclic GMP-gated channels of bovine rod photoreceptors: Affinity, density and stoichiometry of Ca(2+)-calmodulin binding sites. *The Journal of Physiology, 494,* 675–685. [PubMed] [Article]

Baylor, D. A., & Hodgkin, A. L. (1974). Changes in time scale and sensitivity in turtle photoreceptors. *The Journal of Physiology, 242,* 729–758. [PubMed] [Article]

Baylor, D. A., Hodgkin, A. L., & Lamb, T. D. (1974). The electrical response of turtle cones to flashes and steps of light. *The Journal of Physiology, 242,* 685–727. [PubMed] [Article]

Bouguer, M. (1760). *Traité d'optique sur la gradation de la lumière*. Paris: De la Calle.

Boynton, R. M., & Whitten, D. N. (1970). Visual adaptation in monkey cones: Recordings of late receptor potentials. *Science, 170,* 1423–1426. [PubMed]

Burkhardt, D. A. (1994). Light adaptation and photopigment bleaching in cone photoreceptors in situ in the retina of the turtle. *The Journal of Neuroscience, 14,* 1091–1105. [PubMed] [Article]

Burns, M. E., & Baylor, D. A. (2001). Activation, deactivation and adaptation in vertebrate photoreceptor cells. *Annual Review of Neuroscience, 24,* 779–805. [PubMed]

Burns, S. A., & Elsner, A. E. (1985). Color matching at high luminances: The color-match-area effect and photopigment bleaching. *Journal of the Optical Society of America A, Optics and Image Science, 2,* 698–704. [PubMed]

Burns, S. A., & Elsner, A. E. (Eds.) (1989). *Localizing color vision deficiencies in eye disease* (vol. IX). Dordrecht: Kluwer Academic Publishers.

Burton, G. J. (1973). Evidence for non-linear response processes in the human visual system from measurements on the thresholds of spatial beat frequencies. *Vision Research, 13,* 1211–1225. [PubMed]

Carroll, J., Neitz, M., Hofer, H., Neitz, J., & Williams, D. R. (2004). Functional photoreceptor loss revealed with adaptive optics: An alternative cause of color blindness. *Proceedings of the National Academy of Sciences of the United States of America, 101,* 8461–8466. [PubMed] [Article]

Cavonius, C. R. (1979). Binocular interactions in flicker. *The Quarterly Journal of Experimental Psychology, 31,* 273–280. [PubMed]

Cavonius, C. R., & Estévez, O. (1980). Applications of signal-processing methods in visual psychophysics. In M. Kunt & F. de Coulon (Eds.), *Signal processing: Theories and applications* (pp. 343–349). Amsterdam: North-Holland Publishing Company.

Cavonius, C. R., Estévez, O., & van der Tweel, L. H. (1992). Counterphase dichoptic flicker is seen as its own second harmonic. *Ophthalmic & Physiological Optics, 12,* 153–156. [PubMed]

Chen, T. Y., Illing, M., Molday, L. L., Hsu, Y. T., Yau, K. W., & Molday, R. S. (1994). Subunit 2 (or beta) of retinal rod cGMP-gated cation channel is a component of the 240-kDa channel-associated protein and mediates Ca(2+)-calmodulin modulation. *Proceedings of the National Academy of Sciences of*

the United States of America, 91, 11757–11761. [PubMed] [Article]

De Lange, H. (1954). Relationship between critical flicker frequency and a set of low-frequency characteristics of the eye. *Journal of the Optical Society of America, 44,* 380–389.

De Lange, H. (1958). Research into the dynamic nature of the human fovea–cortex systems with intermittent and modulated light: I. Attenuation characteristics with white and colored light. *Journal of the Optical Society of America, 48,* 777–784.

De Lange, H. (1961). Eye's response at flicker fusion to square-wave modulation of a test field surrounded by a large steady field of equal mean luminance. *Journal of the Optical Society of America, 51,* 415–421.

Dowling, J. E., & Ripps, H. (1970). Visual adaptation in the retina of the skate. *The Journal of General Physiology, 56,* 491–520. [PubMed] [Article]

Fain, G. L., Lamb, T. D., Matthews, H. R., & Murphy, R. L. (1989). Cytoplasmic calcium as the messenger for light adaptation in salamander rods. *The Journal of Physiology, 416,* 215–243. [PubMed] [Article]

Fain, G. L., Matthews, H. R., & Cornwall, M. C. (1996). Dark adaptation in vertebrate photoreceptors. *Trends in Neurosciences, 19,* 502–507. [PubMed]

Fain, G. L., Matthews, H. R., Cornwall, M. C., & Koutalos, Y. (2001). Adaptation in vertebrate photoreceptors. *Physiological Reviews, 81,* 117–151. [PubMed] [Article]

Fechner, G. T. (1860). *Elemente der Psychophysik*. Leipzig: Breitkopf and Hartel.

Fuortes, M. G., & Hodgkin, A. L. (1964). Changes in time scale and sensitivity in the ommatidia of limulus. *The Journal of Physiology, 172,* 239–263. [PubMed] [Article]

Geisler, W. S. (1978). Adaptation, afterimages and cone saturation. *Vision Research, 18,* 279–289. [PubMed]

Graham, N., & Hood, D. C. (1992). Modeling the dynamics of light adaptation: The merging of two traditions. *Vision Research, 32,* 1373–1393. [PubMed]

Gray-Keller, M. P., & Detwiler, P. B. (1996). Ca2+ dependence of dark- and light-adapted flash responses in rod photoreceptors. *Neuron, 17,* 323–331. [PubMed]

Green, D. G. (1968). The contrast sensitivity of the colour mechanisms of the human eye. *The Journal of Physiology, 196,* 415–429. [PubMed] [Article]

Grunwald, M. E., Yu, W. P., Yu, H. H., & Yau, K. W. (1998). Identification of a domain on the beta-subunit of the rod cGMP-gated cation channel that mediates inhibition by calcium-calmodulin. *Journal of Biological Chemistry, 273,* 9148–9157. [PubMed] [Article]

Hayhoe, M. M., Benimoff, N. I., & Hood, D. C. (1987). The time course of multiplicative and subtractive adaptation process. *Vision Research, 27,* 1981–1996. [PubMed]

Hecht, S. (1937). Rods, cones and the chemical basis of vision. *Physiological Reviews, 17,* 239–290.

Hodgkin, A. L., & Nunn, B. J. (1988). Control of light-sensitive current in salamander rods. *The Journal of Physiology, 403,* 439–471. [PubMed] [Article]

Hood, D. C. (1998). Lower-level visual processing and models of light adaptation. *Annual Review of Psychology, 49,* 503–535. [PubMed]

Hood, D. C., & Birch, D. G. (1993). Human cone receptor activity: The leading edge of the a-wave and models of receptor activity. *Visual Neuroscience, 10,* 857–871. [PubMed]

Hood, D. C., & Finkelstein, M. A. (1986). Sensitivity to light. In K. Boff, L. Kaufman, & J. Thomas (Eds.), *Handbook of Perception and Human Performance* (vol. 1, pp. 5-1–5-66). New York: Wiley.

Hood, D. C., Finkelstein, M. A., & Buckingham, E. (1979). Psychophysical tests of models of the response function. *Vision Research, 19,* 401–406. [PubMed]

Hood, D. C., Graham, N., von Wiegand, T. E., & Chase, V. M. (1997). Probed-sinewave paradigm: A test of models of light-adaptation dynamics. *Vision Research, 37,* 1177–1191. [PubMed]

Hsu, Y. T., & Molday, R. S. (1993). Modulation of the cGMP-gated channel of rod photoreceptor cells by calmodulin. *Nature, 361,* 76–79. [PubMed]

Hsu, Y. T., & Molday, R. S. (1994). Interaction of calmodulin with the cyclic GMP-gated channel of rod photoreceptor cells. Modulation of activity, affinity purification, and localization. *The Journal of Biological Chemistry, 269,* 29765–29770. [PubMed] [Article]

Ireland, F. H. (1950). A comparison of critical flicker frequencies under conditions of monocular and binocular stimulation. *Journal of Experimental Psychology, 40,* 282–286. [PubMed]

Kelly, D. H. (1961a). Flicker fusion and harmonic analysis. *Journal of the Optical Society of America, 51,* 917–918. [PubMed]

Kelly, D. H. (1961b). Visual response to time-dependent stimuli: I. Amplitude sensitivity measurements. *Journal of the Optical Society of America, 51,* 422–429. [PubMed]

Kelly, D. H. (1964). Sine waves and flicker fusion. *Documenta Ophthalmologica, 18,* 16–35. [PubMed]

Kelly, D. H. (1972). Flicker. In D. Jameson & L. H. Hurvich (Eds.), *Visual psychophysics, handbook of sensory physiology* (vol. VII/4, pp. 273–302). Berlin: Springer-Verlag.

Kelly, D. H. (1974). Spatio-temporal frequency characteristics of color-vision mechanisms. *Journal of the Optical Society of America, 64,* 983–990.

Koutalos, Y., Nakatani, K., Tamura, T., & Yau, K. W. (1995). Characterization of guanylate cyclase activity in single retinal rod outer segments. *The Journal of General Physiology, 106,* 863–890. [PubMed] [Article]

Koutalos, Y., Nakatani, K., & Yau, K.-W. (1995). The cGMP-phosphodiesterase and its contribution to sensitivity regulation in retinal rods. *The Journal of General Physiology, 106,* 891–921. [PubMed] [Article]

Koutalos, Y., & Yau, K. W. (1996). Regulation of sensitivity in vertebrate rod photoreceptors by calcium. *Trends in Neurosciences, 19,* 73–81. [PubMed]

Lamb, T. D., & Pugh, E. N., Jr. (2004). Dark adaptation and the retinoid cycle of vision. *Progress in Retinal and Eye Research, 23,* 307–380. [PubMed]

Lee, B. B., Dacey, D. M., Smith, V. C., & Pokorny, J. (1999). Horizontal cells reveal cone type-specific adaptation in primate retina. *Proceedings of the National Academy of Sciences of the United States of America, 96,* 14611–14616. [PubMed] [Article]

Lee, B. B., Dacey, D. M., Smith, V. C., & Pokorny, J. (2003). Dynamics of sensitivity regulation in primate outer retina: The horizontal cell network. *Journal of Vision, 3*(7), 513–526, http://journalofvision.org/3/7/5/, doi:10.1167/3.7.5. [PubMed] [Article]

Leibrock, C. S., Reuter, T., & Lamb, T. D. (1998). Molecular basis of dark adaptation in rod photoreceptors. *Eye, 12,* 511–520. [PubMed]

Lit, A. (1949). The magnitude of the Pulfrich stereophenomenon as a function of binocular differences of intensity at various levels of illumination. *American Journal of Psychology, 62,* 159–181.

MacLeod, D. I. (1978). Visual sensitivity. *Annual Review of Psychology, 29,* 613–645. [PubMed]

MacLeod, D. I., & He, S. (1993). Visible flicker from invisible patterns. *Nature, 361,* 256–258. [PubMed]

MacLeod, D. I., Williams, D. R., & Makous, W. (1992). A visual nonlinearity fed by single cones. *Vision Research, 32,* 347–363. [PubMed]

Mahroo, O. A., & Lamb, T. D. (2004). Recovery of the human photopic electroretinogram after bleaching exposures: Estimation of pigment regeneration kinetics. *The Journal of Physiology, 554,* 417–437. [PubMed] [Article]

Matin, L. (1968). Critical duration, the differential luminance threshold, critical flicker frequency, and visual adaptation: A theoretical treatment. *Journal of the Optical Society of America, 58,* 404–415. [PubMed]

Matthews, H. R. (1996). Static and dynamic actions of cytoplasmic Ca2+ in the adaptation of responses to saturating flashes in salamander rods. *The Journal of Physiology, 490,* 1–15. [PubMed] [Article]

Matthews, H. R. (1997). Actions of Ca2+ on an early stage in phototransduction revealed by the dynamic fall in Ca2+ concentration during the bright flash response. *The Journal of General Physiology, 109,* 141–146. [PubMed] [Article]

Matthews, H. R., Murphy, R. L. W., Fain, G. L., & Lamb, T. D. (1988). Photoreceptor light adaptation is mediated by cytoplasmic calcium concentration. *Nature, 334,* 67–69. [PubMed]

Merbs, S. L., & Nathans, J. (1992). Absorption spectra of the hybrid pigments responsible for anomalous color vision. *Science, 258,* 464–466. [PubMed]

Murnick, J. G., & Lamb, T. D. (1996). Kinetics of desensitization induced by saturating flashes in toad and salamander rods. *The Journal of Physiology, 495,* 1–13. [PubMed] [Article]

Nikonov, S., Engheta, N., & Pugh, E. N., Jr. (1998). Kinetics of recovery of the dark-adapted salamander rod photoresponse. *The Journal of General Physiology, 111,* 7–37. [PubMed] [Article]

Parinaud, H. (1881). L'héméralopie et les fonctions du pourple visuel. *Comptes rendus hebdomadaires des séances et mémories de la Société de biologie, 93,* 286–287.

Penn, R. D., & Hagins, W. A. (1972). Kinetics of photocurrent of retinal rods. *Biophysical Journal, 12,* 1073–1094. [PubMed] [Article]

Pepperberg, D. R. (2003). Bleaching desensitization: Background and current challenges. *Vision Research, 43,* 3011–3019. [PubMed]

Perlman, I., & Normann, R. A. (1998). Light adaptation and sensitivity controlling mechanisms in vertebrate photoreceptors. *Progress in Retinal and Eye Research, 17,* 523–563. [PubMed]

Perrin, F. H. (1954). A study in binocular flicker. *Journal of the Optical Society of America, 44,* 60–69. [PubMed]

Plateau, J. (1835). Sur un principle de photométrie. *Bulletins de l'Académie royale des sciences et belles-lettres de Bruxelles, 2,* 52–59.

Polans, A., Baehr, W., & Palczewski, K. (1996). Turned on by Ca2+! The physiology and pathology of Ca(2+)-binding proteins in the retina. *Trends in Neurosciences, 19,* 547–554. [PubMed]

Pugh, E. N., Jr., Duda, T., Sitaramayya, A., & Sharma, R. K. (1997). Photoreceptor guanylate cyclases: A review. *Bioscience Reports, 17,* 429–473. [PubMed]

Pugh, E. N., Jr., & Lamb, T. D. (2000). Phototransduction in vertebrate rods and cones: Molecular mechanisms of amplification, recovery and light adaptation. In D. G. Stavenga, W. J. de Grip, & E. N. Pugh (Eds.), *Handbook of biological physics: Vol. 3. Molecular mechanisms of visual transduction* (pp. 183–255). Amsterdam: Elsevier.

Pugh, E. N., Jr., Nikonov, S., & Lamb, T. D. (1999). Molecular mechanisms of vertebrate photoreceptor light adaptation. *Current Opinion in Neurobiology, 9,* 410–418. [PubMed]

Pulfrich, C. (1922). Die Stereskopie im Dienste der isochromen und heterochromen Photemetrie. *Naturwissenschaften, 10,* 553–564, 569–574, 596–601, 714–722, 735–743, 751–761.

Rebrik, T. I., & Korenbrot, J. I. (1998). In intact cone photoreceptors, a Ca2+-dependent, diffusible factor modulates the cGMP-gated ion channels differently than in rods. *The Journal of General Physiology, 112,* 537–548. [PubMed] [Article]

Reeves, A., Wu, S., & Schirillo, J. (1998). The effect of photon noise on the detection of white flashes. *Vision Research, 38,* 691–703. [PubMed]

Rock, M. L., & Fox, B. H. (1949). Two aspects of the Pulfrich phenomenon. *American Journal of Psychology, 62,* 279–284.

Roufs, J. A. (1972a). Dynamic properties of vision: I. Experimental relationships between flicker and flash thresholds. *Vision Research, 12,* 261–278. [PubMed]

Roufs, J. A. (1972b). Dynamic properties of vision: II. Theoretical relationship between flicker and flash thresholds. *Vision Research, 12,* 279–292. [PubMed]

Rushton, W. A. (1963). A cone pigment in the protanope. *The Journal of Physiology, 168,* 345–359. [PubMed] [Article]

Rushton, W. A. (1965). A foveal pigment in the deuteranope. *The Journal of Physiology, 176,* 24–37. [PubMed] [Article]

Schnapf, J. L., Nunn, B. J., Meister, M., & Baylor, D. A. (1990). Visual transduction in cones of the monkey Macaca fascicularis. *The Journal of Physiology, 427,* 681–713. [PubMed] [Article]

Schultze, M. (1866). Zur Anatomie und Physiologie der Retina. *Archiv für mikroskopische Anatomie und Entwicklungsmechanik, 2,* 175–286.

Shapley, R., & Enroth-Cugell, C. (1984). Visual adaptation and retinal gain controls. In N. Osborne & G. Chader (Eds.), *Progress in retinal research* (vol. 3, pp. 263–346). New York: Pergamon Press.

Sharpe, L. T., Stockman, A., Jägle, H., Knau, H., Klausen, G., Reitner, A., et al. (1998). Red, green, and red–green hybrid photopigments in the human retina: Correlations between deduced protein sequences and psychophysically-measured spectral sensitivities. *The Journal of Neuroscience, 18,* 10053–10069. [PubMed] [Article]

Sherrington, C. S. (1906). *The integrative action of the nervous system.* New Haven: Yale University Press.

Smith, V. C., Lee, B. B., Pokorny, J., Martin, P. R., & Valberg, A. (1992). Responses of macaque ganglion cells to the relative phase of heterochromatically modulated lights. *The Journal of Physiology, 458,* 191–221. [PubMed] [Article]

Smith, V. C., Pokorny, J., Lee, B. B., & Dacey, D. M. (2001). Primate horizontal cell dynamics: An analysis of sensitivity regulation in the outer retina. *Journal of Neurophysiology, 85,* 545–558. [PubMed] [Article]

Smith, V. C., Pokorny, J., & van Norren, D. (1983). Densitometric measurement of human cone photopigment kinetics. *Vision Research, 23,* 517–524. [PubMed]

Sperling, G., & Sondhi, M. M. (1968). Model for visual luminance discrimination and flicker detection. *Journal of the Optical Society of America, 58,* 1133–1145. [PubMed]

Stockman, A., MacLeod, D. I., & Lebrun, S. J. (1993). Faster than the eye can see: Blue cones respond to rapid flicker. *Journal of the Optical Society of America A, Optics and Image Science, 10,* 1396–1402. [PubMed]

Stockman, A., & Plummer, D. J. (2005a). Long-wavelength adaptation reveals slow, spectrally opponent inputs to the human luminance pathway. *Journal of Vision, 5*(9), 702–716, http://journalofvision.org/5/9/5/, doi:10.1167/5.9.5. [PubMed] [Article]

Stockman, A., & Plummer, D. J. (2005b). Spectrally-opponent inputs to the human luminance pathway: slow +L and −M cone inputs revealed by low to moderate long-wavelength adaptation. *The Journal of Physiology, 566,* 77–91. [PubMed] [Article]

Stockman, A., Plummer, D. J., & Montag, E. D. (2005). Spectrally opponent inputs to the human luminance pathway: Slow +L and −M cone inputs revealed by intense long-wavelength adaptation. *The Journal of Physiology, 566,* 61–76. [PubMed] [Article]

Stockman, A., & Sharpe, L. T. (2000). Spectral sensitivities of the middle- and long-wavelength sensitive cones derived from measurements in observers of known genotype. *Vision Research, 40,* 1711–1737. [PubMed]

Stromeyer, C. F., III, Gowdy, P. D., Chaparro, A., Kladakis, S., Willen, J. D., & Kronauer, R. E.

(2000). Colour adaptation modifies the temporal properties of the long- and middle-wave cone signals in the human luminance mechanism. *The Journal of Physiology, 526,* 177–194. [PubMed] [Article]

Talbot, H. F. (1834). Experiments on light. *Philosophical Magazine Series 3, 5,* 321–334.

Tamura, T., Nakatani, K., & Yau, K. W. (1991). Calcium feedback and sensitivity in primate rods. *The Journal of General Physiology, 98,* 95–130. [PubMed] [Article]

Thomas, G. J. (1954). The effect on critical flicker frequency of interocular differences in intensity and in phase relations of flashes of light. *The American Journal of Psychology, 67,* 632–646. [PubMed]

Thomas, G. J. (1955). A comparison of uniocular and binocular critical flicker frequencies: simultaneous and alternate flashes. *The American Journal of Psychology, 68,* 37–53. [PubMed]

Thomas, G. J. (1956). Effect of contours on binocular CFF obtained with synchronous and alternate flashes. *The American Journal of Psychology, 69,* 369–377. [PubMed]

Torre, V., Matthews, H. R., & Lamb, T. D. (1986). Role of calcium in regulating the cyclic GMP cascade of phototransduction in retinal rods. *Proceedings of the National Academy of Sciences of the United States of America, 83,* 7109–7113. [PubMed] [Article]

Tranchina, D., Gordon, J., & Shapley, R. M. (1984). Retinal light adaptation—Evidence for a feedback mechanism. *Nature, 310,* 314–316. [PubMed]

Valeton, J. M., & van Norren, D. (1983). Light adaptation of primate cones: An analysis based on extracellular data. *Vision Research, 23,* 1539–1547. [PubMed]

van Hateren, H. (2005). A cellular and molecular model of response kinetics and adaptation in primate cones and horizontal cells. *Journal of Vision, 5*(4), 331–347, http://journalofvision.org/5/4/5/, doi:10.1167/5.4.5. [PubMed] [Article]

von Kries, J. (1894). Über den Einfluß der Adaptation auf Licht- und Farbenempfindung und über die Funktion der Stäbchen. *Bericht der naturforschungs Gesellschaft, Freiburg im Breisgau, 9,* 61–70.

von Kries, J. (1896). Über die Funktion der Netzhautstäbchen. *Zeitschrift für Psychologie und Physiologie der Sinnesorgane, 9,* 81–123.

von Kries, J. (1902). Theoretische studien über die Umstimmung des Sehorgans. *Festschrift der Albrecht-Ludwig-Universität.* English translation by MacAdam, D. L. (1970). *Sources of color science* (pp. 109–119). Cambridge: MIT Press.

von Wiegand, T. E., Hood, D. C., & Graham, N. (1995). Testing a computational model of light-adaptation dynamics. *Vision Research, 35,* 3037–3051. [PubMed]

Watson, A. B. (1986). Temporal sensitivity. In K. Boff, L. Kaufman, & J. Thomas (Eds.), *Handbook of perception and human performance* (vol. 1, pp. 6-1–6-43). New York: Wiley.

Weitz, D., Zoche, M., Muller, F., Beyermann, M., Korschen, H. G., Kaupp, U. B., et al. (1998). Calmodulin controls the rod photoreceptor CNG channel through an unconventional binding site in the N-terminus of the beta-subunit. *The European Molecular Biology Organization Journal, 17,* 2273–2284. [PubMed] [Article]

Whitlock, G. G., & Lamb, T. D. (1999). Variability in the time course of single photon responses from toad rods: Termination of rhodopsin's activity. *Neuron, 23,* 337–351. [PubMed] [Article]

Wilson, J. A., & Anstis, S. M. (1969). Visual delay as a function of luminance. *The American Journal of Psychology, 82,* 350–358. [PubMed]